

Efficient Gaussian Process Classification-based Physical-Layer Authentication with Configurable Fingerprints for 6G-Enabled IoT

Rui Meng, *Graduate Student Member, IEEE*, Fangzhou Zhu, Xiaodong Xu, *Senior Member, IEEE*,
Liang Jin, Bizhu Wang, Bingxuan Xu, Han Meng, and Ping Zhang, *Fellow, IEEE*

Abstract—Physical-Layer Authentication (PLA) has been recently believed as an endogenous-secure and energy-efficient technique to recognize IoT terminals. However, the major challenge of applying the state-of-the-art PLA schemes directly to 6G-enabled IoT is the inaccurate channel fingerprint estimation in low Signal-Noise Ratio (SNR) environments, which will greatly influence the reliability and robustness of PLA. To tackle this issue, we propose a configurable-fingerprint-based PLA architecture through Intelligent Reflecting Surface (IRS) that helps create an alternative wireless transmission path to provide more accurate fingerprints. According to Baye’s theorem, we propose a Gaussian Process Classification (GPC)-based PLA scheme, which utilizes the Expectation Propagation (EP) method to obtain the identities of unknown fingerprints. Considering that obtaining sufficient labeled fingerprint samples to train the GPC-based authentication model is challenging for future 6G systems, we further extend the GPC-based PLA to the Efficient-GPC (EGPC)-based PLA through active learning, which requires fewer labeled fingerprints and is more feasible. We also propose three fingerprint selecting algorithms to choose fingerprints, whose identities are queried to the upper-layers authentication mechanisms. For this reason, the proposed EGPC-based scheme is also a lightweight cross-layer authentication method to offer a superior security level. The simulations conducted on synthetic datasets demonstrate that the IRS-assisted scheme reduces the authentication error rate by 98.69% compared to the non-IRS-based scheme. Additionally, the proposed fingerprint selection algorithms reduce the authentication error rate by 65.96% to 86.93% and 45.45% to 70.00% under perfect and imperfect channel estimation conditions, respectively, when compared with baseline algorithms.

Index Terms—Physical-Layer Authentication (PLA), 6G, IoT, identity security, Intelligent Reflecting Surface (IRS).

I. INTRODUCTION

A. Background

This work was supported in part by the National Key R&D Program of China under Grant 2020YFB1806900 and in part by the Fundamental Research Foundation for the Central Universities under Grant 2022RC15. (*Corresponding author: Xiaodong Xu*)

Rui Meng, Fangzhou Zhu, Liang Jin, Bizhu Wang, and Bingxuan Xu are with the State Key Laboratory of Networking and Switching Technology, Beijing University of Posts and Telecommunications, Beijing 100876, China (e-mail: buptmengrui@bupt.edu.cn; zfz9941@bupt.edu.cn; jin-liang@bupt.edu.cn; wangbizhu_7@bupt.edu.cn; xubingxuan@bupt.edu.cn).

Xiaodong Xu and Ping Zhang are with the State Key Laboratory of Networking and Switching Technology, Beijing University of Posts and Telecommunications, Beijing 100876, China, and also with the Department of Broadband Communication, Peng Cheng Laboratory, Shenzhen 518066, Guangdong, China (e-mail: xuxiaodong@bupt.edu.cn; pzhang@bupt.edu.cn).

Han Meng is with the Key Laboratory of Universal Wireless Communication, Beijing University of Posts and Telecommunications, Beijing 100876, China (email: menghan@bupt.edu.cn).

AS AN extended and expanded system network based on the Internet, Internet of Things (IoT) can realize intelligent perception, recognition, and management of things and machine leveraging various devices and technologies, such as sensor equipment, global positioning system, infrared sensor, and laser scanner [1]. Through network slicing, millimeter-wave transmission, and massive multi-input and multi-output (MIMO) architecture, the 5th generation mobile network (5G) has empowered IoT to connect more things, thus presenting more imagination and application space for various industries. However, due to the remarkable surge in smart device adoption and the rapid growth of IoT networks, the capabilities of 5G alone may not be sufficient to meet the increasingly demanding technical requirements. For instance, the need for autonomous, highly dynamic, strongly secure, and fully intelligent services cannot be completely fulfilled by 5G [2], [3]. To support the ultimate goal of IoT, that is, real-time interaction between things, machines, and people, the 6th generation mobile network (6G) will provide improved services in terms of seamless coverage, data rate, and endogenous security. This will be accomplished through the implementation of multi-band ultrafast-speed transmission, a highly adaptable integrated network, multi-node multi-domain joint transmission, and intelligent transmission mechanisms [4], [5].

Nevertheless, the worldwide seamless integration of IoT enabled by 6G necessitates an increased involvement of radio equipment in communication processes. This expansion of the application field, however, also introduces heightened security risks of a more pressing nature [4]. Besides, owing to the wireless transmission media’s open broadcast nature, more aggressors may fabricate identification information to pretend to be legitimate users and further modify their privacy information [6]. Hence, the lightweight and efficient identity authentication plays a crucial role in achieving seamless and trustworthy communication [7]. Currently, the identity identification of terminals in 5G systems is mainly achieved by the core network, which adopts the authentication mechanisms based on cryptography, such as 5G Authentication and Key Agreement (5G AKA) [8]. Although the above cryptographic techniques at the upper layers have been incorporated into the 5G standard and have been commercially available, they will fail to meet the expected performance levels in various emerging applications integrating 6G and IoT due to the following limitations.

- First of all, the security level of the aforementioned identification architectures is constrained due to their reliance on the assumption that adversaries possess finite computational resources [9]. For example, quantum computing poses a significant threat to security authentication algorithms based on cryptography. With the potential to perform complex calculations at an unprecedented speed, quantum computers have the capability to break traditional cryptographic algorithms that rely on the difficulty of factoring large numbers or solving discrete logarithm problems. This means that widely used encryption methods, such as Rivest, Shamir, and Adleman (RSA) and elliptic curve cryptosystems (ECCs), could be rendered ineffective against attacks by quantum computers [10].
- Secondly, in the context of 6G, achieving global seamless coverage is a crucial goal. However, due to the differences between devices and systems, existing 5G identity authentication protocols may not run seamlessly on all devices. Therefore, it is urgent to explore and develop new identity authentication protocols and mechanisms that are suitable for heterogeneous networks, can cross different devices and systems, provide consistent identity authentication experiences, and ensure that all devices in the network can perform secure authentication [11].
- Thirdly, traditional cryptography techniques require the generation, distribution, and refresh of keys, thus greatly increasing the transmission latency, which makes it challenging to perform well in latency-sensitive applications, such as smart hospitals [12]. Besides, it is difficult for most IoT terminals with limited resources to bear the computational overhead of storing the upper-layers identification protocols [13].

Consequently, to ensure high-reliable communication in 6G-enabled IoT, more efficient and reliable terminal access recognition approaches are required.

B. Physical-Layer Authentication (PLA)

To effectively address the aforementioned limitations of upper-layers security mechanisms, Physical-Layer Authentication (PLA) has recently emerged as a complement of traditional security mechanisms and a promising identity authentication approach for 6G systems, offering the following strengths.

- First of all, unlike the “patch” and “plugin” cryptography techniques at the upper-layers [14], PLA is designed based on physical-layer features that are exploited from the communication links, devices, and location-related attributes [9], [13], [15], such as Channel State Information (CSI) [16], [17], Received Signal Strength (RSS) [6], [12], peak power (PP) [6], [18], Channel Impulse Response (CIR) [12], [13], and Channel Frequency Response (CFR) [19], [20]. These physical quantities are regarded as inherent fingerprints, possessing unique characteristics such as temporal variability, randomness, and spatial independence within radio channels [14], [17]. More specifically, the endogenous fingerprints of two transmitters situated at a half-wavelength distance

can be considered completely independent in terms of time, frequency, and spatial factors [15]. That is to say, endogenous fingerprints at the physical-layer can provide particular identifying signatures and natural dynamic protection for legitimate IoT terminals, and extracting these channel characteristics and forging them presents an immensely formidable challenge for adversaries [13].

- Besides, PLA is a lightweight method circumventing many upper-layer signaling processes, leading to improved efficiency. Furthermore, during the channel estimation phase, the access point obtains the CSI of all authorized users, which further reduces computational overhead. Consequently, IoT devices with limited computing and storage resources can perform optimally [9].
- In addition, PLA utilizes the physical-layer characteristics of devices for identification and verification, independent of software and protocols. It ensures a consistent experience through unified authentication standards, customizable to specific needs. It is suitable for heterogeneous network environments and provides identity authentication for different devices [21].

In earlier literature, PLA is formulated as the statistical hypothesis testing [22]–[24]. To be specific, the estimated fingerprints are identified as legitimate when the differences between them and the reference vector do not exceed the detection threshold. However, owing to the challenges in accurately modeling the fingerprints of IoT terminals caused by unknown and uncertain dynamic variation in 6G systems, it is difficult for the threshold judgement-based PLA schemes to obtain the theoretical optimal threshold [25].

More recently, Machine Learning (ML)-based PLA approaches have attracted more interest to improve the reliability and robustness of access authentication [26]. Through exploring ML techniques, such as Gaussian kernel method [25], Support Vector Machine (SVM) [27], weighted voting [28], neural networks [17], [20], [29], and Reinforcement Learning (RL) [30], the data-driven PLA is formulated as a classification problem, thereby realizing threshold-free and improving identification efficiency [31].

C. Challenges

The first challenge is the inaccurate channel fingerprint estimation. As important identifying signatures of IoT terminals, endogenous fingerprints should be high-accurate to present significantly distinguishable features for different transmitters. However, some low Signal-Noise Ratio (SNR) environments in 6G systems, such as noises and user movements, will interfere with the precise estimation of channel fingerprints, which will obviously limit the identification performance [21]. To tackle this challenge, one feasible approach is the multi-attribute [6], [12], [32] and multi-observation [19] [28], [33] to provide multi-dimensional identity characteristics of transmitters. The restricted range of the single fingerprint distribution contributes to the diminished reliability of identification. In contrast, multi-attribute or multi-observation can provide additional recognizability for legal IoT terminals to mitigate the bias of each. Thus, the spoofing attackers will have more

challenges in predicting and forging legal fingerprints [6], [12]. However, when the direct paths between the transmitter and receiver are blocked, the multi-attribute-based approaches can not effectively enhance the authentication performance. Although the multi-observation-based methods can address this issue by alternative direct paths of additional receivers, the deployment cost and security of multi-receivers need to be further considered.

The second challenge is the dependence on expert databases. Training Supervised Learning (SL)-based PLA models requires the prior information of legitimate terminals and spoofing attackers as guiding. Unfortunately, given the dynamic nature of wireless environments and the frequent occurrence of short signaling interactions in 6G systems, acquiring attackers' training fingerprints and describing its probability distribution prove to be challenging [6]. To address this challenge, many researchers have proposed several PLA schemes based on Unsupervised Learning (UL), such as kernel machine [12], variational autoencoder [16], clustering [6], and one-class classifier (OCC) [19], [27]. Such PLA schemes are achieved without requiring the prior information of attackers. In fact, the performance of ML-based PLA models is influenced by the prior information of fingerprint samples, that is, the more prior information of fingerprints, the higher accuracy of ML-based authentication models. Hence, designing an appropriate ML-aided authentication process that more effectively utilizes the limited prior information available to attackers, to achieve highly reliable identity authentication, is an urgent problem that needs to be solved.

D. Our Solutions

Against this background, to tackle the first challenge, we propose a configurable-fingerprint-based PLA architecture leveraging Intelligent Reflecting Surface (IRS), which can help create an alternative transmission path with better channel quality. Particularly, IRS is a groundbreaking physical-layer technology for 6G that employs a planar array of cost-effective reflective elements to dynamically manipulate the phase, amplitude, or frequency of incoming signals, thereby enhancing the overall communication performance [34]. Currently, extensive exploration is being conducted on integrating IRSs into forthcoming 6G networks. IRSs would be primarily controlled by base stations (BSs) for the purpose of augmenting coverage, particularly in high-frequency ranges like millimeter waves. It is worth noting that these deployments have the potential to be utilized for authentication purposes as well.

To tackle the second challenge, we propose an active learning-based PLA scheme, which requires fewer labeled fingerprint samples. Active learning is a specialized subfield within human-in-the-loop machine learning methods, where humans take on an "omniscient" role and hand-label specific data points [35]. Both empirical studies and theoretical analyses have demonstrated that active learning, by carefully selecting data for labeling, can attain similar accuracy with fewer labeled instances compared to classic ML algorithms [36]. For the ML-based PLA approaches, obtaining unlabeled fingerprint samples is less costly than acquiring labeled fingerprint samples. However, not all fingerprint samples are equally

valuable for learning the distribution of fingerprints. Hence, the active learning-aided PLA scheme can reduce the cost of obtaining labeled fingerprints.

E. Contributions

To provide a concise summary, the primary contributions can be outlined as follows:

- We propose a lightweight cross-layer PLA architecture aided by IRS to achieve highly reliable and efficient identity authentication for 6G-enabled IoT. The configurable fingerprints are obtained with the help of IRS, which can create an alternative transmission path, to enhance the reliability of fingerprints when the channel quality between Alice and Bob is poor or even the direct link is blocked.
- We propose a Gaussian Process Classification (GPC)-based PLA scheme upon the designed IRS-aided PLA architecture. We further use the Expectation Propagation (EP) method to obtain the approximated posterior prediction of the identity of unknown configurable fingerprints.
- We combine active learning and PLA to propose the Efficient-GPC (EGPC)-based PLA scheme, including a fingerprint select query, interaction with the upper-layer authentication mechanisms, and the GPC-based PLA model, to improve the efficiency of fingerprint labeling. We further propose three fingerprint selecting algorithms, including Random Optimization (RO) algorithm, Average Loss of Uncertainty (ALU) algorithm, and Soft-ALU (SALU) algorithm, to select the most uncertain fingerprint sample from the pool of unlabeled fingerprint samples for labeling.
- The simulations on synthetic dataset demonstrates the effectiveness of IRS in reducing authentication error rate. Furthermore, the proposed schemes are shown to outperform baseline active learning algorithms in terms of authentication performance, both in cases of perfect and imperfect channel estimation conditions.

II. SYSTEM MODEL AND PROBLEM FORMULATION

A. Network Model

A typical security model is shown in Fig. 1, where Bob denotes the BS that exclusively controls IRS, thereby having control over the channel to the legal IoT terminal (Alice). Eve represents an spoofing attacker device within the cell and attempts to impersonate Alice via transmitting signals to Bob. We consider that there is no direct links between transmitters and Bob. Hence, IRS can enable the wireless connection between them, thus enhancing the channel quality. By adjusting the configuration of IRS, Bob can manipulate the channel to Alice as desired. The integration of IRSs into authentication protocols holds immense potential, particularly in controlled environments like smart factories [37]. By incorporating IRSs into authentication processes, enhanced security measures can be achieved, ensuring reliable identity verification and access control [38]. This innovative use of IRSs in authentication protocols offers promising possibilities for safeguarding critical systems and assets in various industries.

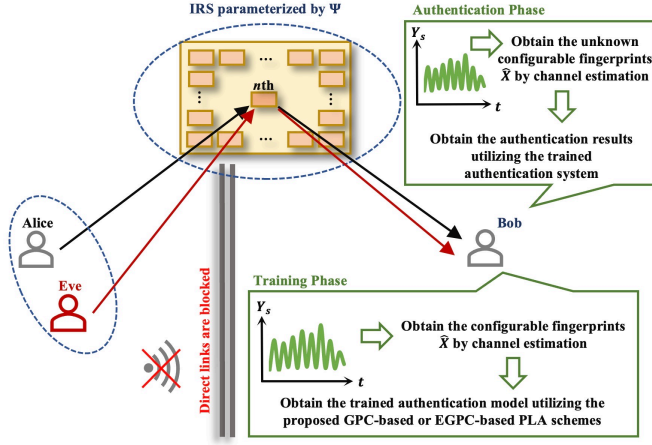


Fig. 1. The designed IRS-assisted authentication framework, where Alice and Eves respectively are legal and spoofing transmitters, and Bob recognizes the identity according to the estimated configurable fingerprints.

B. The Estimation of Configurable Fingerprints

Let N_T and N_R denote the number of antennas of Alice and Bob, respectively. The received signal vector with N_R -size column \mathbf{Y}_S at Bob can be represented as

$$\mathbf{Y}_S = \mathbf{Q}^{(A,I,B)} \mathbf{X}_S + \mathbf{W} \quad (1)$$

where \mathbf{X}_S is the signal vector with N_T -size column transmitted from Alice and $\mathbf{W} \sim \mathcal{CN}(0, \sigma^2)$ is the Gaussian noise vector with N_R -size column. Denoting the number of elements of IRS by N , $\mathbf{Q}^{(A,I,B)} = \mathbf{H}\Psi\mathbf{G}$ is the hierarchical channel matrix from Alice to Bob through IRS, where \mathbf{H} and \mathbf{G} represent the channel matrix with $N_R \times N$ from IRS to Bob and the channel matrix with $N \times N_T$ from Alice to IRS, respectively. $\Psi = \text{diag}(\psi_0, \dots, \psi_{N-1})$ is the matrix of IRS element responses. Each φ_n can be represented as

$$\psi_n = A_n(\theta_n) e^{j\theta_n} \quad (2)$$

where $A_n(\theta_n)$ and $e^{j\theta_n}$ denote the controllable magnitude and phase response of the n th IRS element, respectively. According to [39], we can obtain

$$A_n(\theta_n) = (1 - A_{\min}) \left(\frac{\sin(\theta_n - \Omega) + 1}{2} \right)^v + A_{\min} \quad (3)$$

where A_{\min} is the minimum amplitude, Ω is the horizontal distance, and v affects the steepness of the function curve.

Definition 1. The configurable fingerprints are obtained through channel estimation that is based on a pre-known pilot signal transmitted from Alice, and this process can be mathematically represented as

$$\hat{\mathbf{X}} = \mathbf{Y}_S \mathbf{X}_p^{-1} \quad (4)$$

where \mathbf{X}_p is the $N_T \times N_T$ matrix of the N_T pilot vectors and \mathbf{Y}_S is the $N_R \times N_T$ matrix. As the vital identifying signatures of IoT devices, the configurable fingerprints $\hat{\mathbf{X}}$ can provide significantly distinguishable features for Alice and Eve.

C. Problem Formulation

Proposition 1. For simplicity, we pre-process $\hat{\mathbf{X}}$ and then obtain the $2N_R N_T$ -dimensional real vector \mathbf{x} . Thus, the identity recognition problem can be formulated as a classification function $c(\mathbf{x})$ that assigns the configurable fingerprints \mathbf{x} to one of two classes, $y = 0$ and $y = 1$, corresponding to Alice and Eve, respectively. Specifically, the optimization of the expected loss can be approximated as follows:

$$R_{\mathcal{L}}(c) = \int \mathcal{L}(y, c(\mathbf{x})) p(y, \mathbf{x}) dy d\mathbf{x} \quad (5)$$

Considering that the joint probability $p(y, \mathbf{x})$ is unknown, one natural approach is to decompose $p(y, \mathbf{x})$ as $p(\mathbf{x})p(y|\mathbf{x})$ according to Bayes' theorem, which will be discussed in Section III.

III. PROPOSED GPC-BASED PLA SCHEME

A. Gaussian Process (GP) for PLA

Denote the configurable fingerprint space and the identity label set by \mathcal{X} and $\mathcal{Y} = 0, 1$, respectively. Our purpose is to train an authentication system $\psi: \mathcal{X} \rightarrow \mathcal{Y}$ to estimate the identities of unknown fingerprints $\psi(\mathbf{x}_*)$, $\mathbf{x}_* \in \mathcal{X}$. We use a GPC framework to connect the configurable fingerprints and the identity labels via a latent function f following a GP prior $f \sim GP(\mu(\cdot), k(\cdot, \cdot))$, where $\mu(\cdot)$ and $k(\cdot, \cdot)$ are the mean function and covariance kernel function, respectively.

By ‘‘squashing’’ the GP prior function $f(\mathbf{x})$, we can obtain a prior on $\pi(\mathbf{x})p(y = +1 | \mathbf{x}) = \sigma(f(\mathbf{x}))$ through the logistic function. $f(\mathbf{x})$ can help formulate the model conveniently.

To remove (integrate out) $f(\mathbf{x})$, the distribution of the latent variable of an unknown configurable fingerprint is computed as

$$p(f_* | X, \mathbf{y}, \mathbf{x}_*) = \int p(f_* | X, \mathbf{x}_*, \mathbf{f}) p(\mathbf{f} | X, \mathbf{y}) d\mathbf{f} \quad (6)$$

where $p(\mathbf{f} | X, \mathbf{y}) = p(\mathbf{y} | \mathbf{f}) p(\mathbf{f} | X) / p(\mathbf{y} | X)$ denotes the posterior over the hidden variables. Then, we can use $p(f_* | X, \mathbf{y}, \mathbf{x}_*)$ to obtain the probabilistic prediction of the identity as

$$\bar{\pi}_* \triangleq p(y_* = +1 | X, \mathbf{y}, \mathbf{x}_*) = \int \sigma(f_*) p(f_* | X, \mathbf{y}, \mathbf{x}_*) df_* \quad (7)$$

The integral in (6) and (7) are analytically intractable because of the non-Gaussian likelihood. EP method [40] is utilized to get the approximated non-Gaussian joint posterior.

B. Posterior Prediction of Unknown Fingerprints

According to Bayes' rule, the posterior $p(\mathbf{f} | X, \mathbf{y})$ is denoted as

$$p(\mathbf{f} | X, \mathbf{y}) = \frac{1}{Z} p(\mathbf{f} | X) \prod_{i=1}^n p(y_i | f_i) \quad (8)$$

where $p(\mathbf{f} | X)$ denotes the Gaussian prior, $\prod_{i=1}^n p(y_i | f_i)$ represents the likelihood, and n is the number of the training fingerprint samples. We can obtain marginal likelihood as

$$Z = p(\mathbf{y} | X) = \int p(\mathbf{f} | X) \prod_{i=1}^n p(y_i | f_i) d\mathbf{f} \quad (9)$$

To make $p(\mathbf{f}|X, \mathbf{y})$ analytically intractable, we utilize the probit likelihood as

$$p(y_i|f_i) = \Phi(f_i y_i) \quad (10)$$

where $\Phi(z) = \int_{-\infty}^z \mathcal{N}(x|0, 1)dx$ is the cumulative density function (CDF) of the standard Gaussian distribution. The likelihood $\Phi(f_i y_i)$ is approximated through the local likelihood approximation as

$$p(y_i|f_i) \simeq t_i \left(f_i \left| \tilde{Z}_i, \tilde{\mu}_i, \tilde{\sigma}_i^2 \right. \right) = \tilde{Z}_i \mathcal{N}(f_i | \tilde{\mu}_i, \tilde{\sigma}_i^2) \quad (11)$$

where \tilde{Z}_i , $\tilde{\mu}_i$, and $\tilde{\sigma}_i^2$ are site parameters, and the local likelihoods t_i satisfy

$$\prod_{i=1}^n t_i \left(f_i \left| \tilde{Z}_i, \tilde{\mu}_i, \tilde{\sigma}_i^2 \right. \right) = \mathcal{N}(\tilde{\boldsymbol{\mu}}, \tilde{\Sigma}) \prod_i \tilde{Z}_i \quad (12)$$

where $\tilde{\boldsymbol{\mu}}$ denotes the vector of $\tilde{\mu}_i$ and $\tilde{\Sigma}$ is diagonal with $\tilde{\Sigma}_{ii} = \tilde{\sigma}_i^2$.

We can approximate the posterior of $p(\mathbf{f}|X, \mathbf{y})$ as

$$q(\mathbf{f}|X, \mathbf{y}) \triangleq \frac{1}{Z_{EP}} p(\mathbf{f}|X) \prod_{i=1}^n t_i \left(f_i \left| \tilde{Z}_i, \tilde{\mu}_i, \tilde{\sigma}_i^2 \right. \right) = \mathcal{N}(\boldsymbol{\mu}, \Sigma) \quad (13)$$

where $\boldsymbol{\mu} = \Sigma \tilde{\Sigma}^{-1} \tilde{\boldsymbol{\mu}}$ and $\Sigma = (K^{-1} + \tilde{\Sigma}^{-1})^{-1}$. K is a $n \times n$ covariance matrix. $Z_{EP} = q(\mathbf{y}|X)$ denotes the approximation to Z from (8) and (9).

To choose the parameters of t_i , one feasible approach is to minimize the reversed Kullback-Leibler (KL) divergence $KL(q(\mathbf{f}|X, \mathbf{y}) || p(\mathbf{f}|X, \mathbf{y}))$ with respect to $q(\mathbf{f}|X, \mathbf{y})$, which is also known as the variational inference for GPC. The EP method is used to update the approximation of t_i sequentially, which are discussed as follows.

1) *Marginal Cavity Distribution*: By combining $p(\mathbf{f}|X)$ and $\prod_{i=1}^n t_i \left(f_i \left| \tilde{Z}_i, \tilde{\mu}_i, \tilde{\sigma}_i^2 \right. \right)$, we can obtain the cavity distribution as

$$q_{-i}(f_i) \propto \int p(\mathbf{f}|X) \prod_{j \neq i} t_j \left(f_j \left| \tilde{Z}_j, \tilde{\mu}_j, \tilde{\sigma}_j^2 \right. \right) df_j \quad (14)$$

We combine $p(\mathbf{f}|X)$ and the $(n-1)$ approximate likelihoods in (14) through equivalently removing $t_i \left(f_i \left| \tilde{Z}_i, \tilde{\mu}_i, \tilde{\sigma}_i^2 \right. \right)$ from the approximated posterior $\prod_{i=1}^n t_i \left(f_i \left| \tilde{Z}_i, \tilde{\mu}_i, \tilde{\sigma}_i^2 \right. \right)$ in (13).

Proposition 2. *We can obtain the marginal distribution for f_i from $q(\mathbf{f}|X, \mathbf{y})$ as*

$$q(f_i|X, \mathbf{y}) = \mathcal{N}(f_i | \mu_i, \sigma_i^2) \quad (15)$$

where $\sigma_i^2 = \Sigma_{ii}$.

Proof: See Appendix A. ■

Proposition 3. *Through dividing (15) by t_i , we can obtain the cavity distribution as*

$$q_{-i}(f_i) = \mathcal{N}(f_i | \mu_{-i}, \sigma_{-i}^2) \quad (16)$$

where $\mu_{-i} = \sigma_{-i}^2 (\sigma_i^{-2} \mu_i - \tilde{\sigma}_i^{-2} \tilde{\mu}_i)$ and $\sigma_{-i}^2 = (\sigma_i^{-2} - \tilde{\sigma}_i^{-2})^{-1}$.

Proof: See Appendix B. ■

2) *The Gaussian Approximation to the Non-Gaussian Marginal Distribution*: The product of $q_{-i}(f_i)$ and $p(y_i|f_i)$ can be approximated by a non-normalized Gaussian marginal distribution, which is defined as

$$\hat{q}(f_i) \triangleq \hat{Z}_i \mathcal{N}(\hat{\mu}_i, \hat{\sigma}_i^2) \simeq q_{-i}(f_i) p(y_i|f_i) \quad (17)$$

Proposition 4. *Considering that $\hat{q}(f_i)$ is un-normalized, to match $q_{-i}(f_i) p(y_i|f_i)$, the desired posterior marginal moments should satisfy*

$$\hat{Z}_i = \Phi(z_i) \quad (18)$$

$$\hat{\mu}_i = \mu_{-i} + \frac{y_i \sigma_{-i}^2 \mathcal{N}(z_i)}{\Phi(z_i) \sqrt{1 + \sigma_{-i}^2}} \quad (19)$$

$$\hat{\sigma}_i^2 = \sigma_{-i}^2 - \frac{\sigma_{-i}^4 \mathcal{N}(z_i)}{(1 + \sigma_{-i}^2) \Phi(z_i)} \left(z_i + \frac{\mathcal{N}(z_i)}{\Phi(z_i)} \right) \quad (20)$$

where $z_i = \frac{y_i \mu_{-i}}{\sqrt{1 + \sigma_{-i}^2}}$.

Proof: See Appendix C. ■

3) *The Computation of t_i* :

Proposition 5. *multiplying $\hat{q}(f_i) = \hat{Z}_i \mathcal{N}(\hat{\mu}_i, \hat{\sigma}_i^2)$ by $q_{-i}(f_i) = \mathcal{N}(f_i | \mu_{-i}, \sigma_{-i}^2)$, the site parameters of $p(y_i|f_i) \simeq \tilde{Z}_i \mathcal{N}(f_i | \tilde{\mu}_i, \tilde{\sigma}_i^2)$ in (11) are obtained as*

$$\tilde{\mu}_i = \tilde{\sigma}_i^2 (\tilde{\sigma}_i^{-2} \hat{\mu}_i - \sigma_{-i}^{-2} \mu_{-i}) \quad (21)$$

$$\tilde{\sigma}_i^2 = (\hat{\sigma}_i^{-2} - \sigma_{-i}^{-2})^{-1} \quad (22)$$

$$\tilde{Z}_i = \hat{Z}_i \sqrt{2\pi} \sqrt{\sigma_{-i}^2 + \tilde{\sigma}_i^2} \exp \left(\frac{(\mu_{-i} - \tilde{\mu}_i)^2}{2(\sigma_{-i}^2 + \tilde{\sigma}_i^2)} \right) \quad (23)$$

Proof: See Appendix D. ■

Thus, through iteratively moment matching marginal posteriors, we can approximate $p(\mathbf{f}|X, \mathbf{y})$ with the Gaussian approximation $q(\mathbf{f}|X, \mathbf{y})$.

Proposition 6. *There exists a closed-form expression for $p(y_*|X, \mathbf{y}, \mathbf{x}_*)$ as*

$$p(y_*|X, \mathbf{y}, \mathbf{x}_*) = \Phi \left(\frac{\mathbf{k}_*^T (K + \tilde{\Sigma})^{-1} \tilde{\boldsymbol{\mu}}}{\sqrt{1 + k(\mathbf{x}_*, \mathbf{x}_*) - \mathbf{k}_*^T (K + \tilde{\Sigma})^{-1} \mathbf{k}_*}} \right) \quad (24)$$

where $\mathbf{k}_* = K(X, \mathbf{x}_*)$, \mathbf{k}_*^T denotes the transpose of \mathbf{k}_* , and $k(\mathbf{x}_*, \mathbf{x}_*)$ represents covariance functions evaluated at \mathbf{x}_* and \mathbf{x}_* .

Proof: See Appendix E. ■

Given $p(y_*|X, \mathbf{y}, \mathbf{x}_*)$, we can obtain the identity of unknown fingerprints \mathbf{x}_* according to $\arg \max_{\mathbf{y}_*} p(y_*|X, \mathbf{y}, \mathbf{x}_*)$ [41].

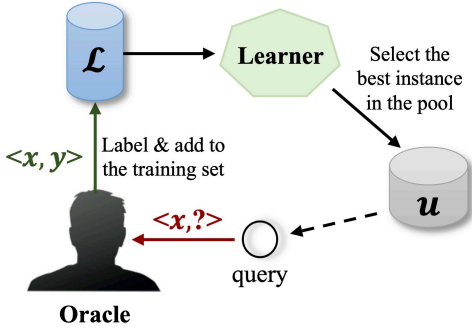


Fig. 2. Illustration of the pool-based active learning.

IV. PROPOSED EGPC-BASED PLA SCHEME

A. Active Learning

The ML techniques can be categorized into SL and UL according to whether the training datasets are labeled. The SL models can obtain better performance than UL models due to the abundant prior information provided by the labels, but the labels are usually difficult to get in practical applications. To tackle the problem, active learning can perform better than UL algorithms with fewer labeled training fingerprint samples than SL algorithms, if it is allowed to choose the data from which it learns. Here, we mainly introduce the pool-based active learning as follows.

As illustrated in Fig. 2, the pool-based active learning usually assumes the availability of a small set of labeled data \mathcal{L} and a large pool of unlabeled data \mathcal{U} . The learner can pose “queries”, usually in the form of unlabeled samples to be labeled by an “oracle”, such as a human annotator. Queries are selected in a greedy manner based on a utility measure that evaluates all unlabeled samples in the pool. The pool-based active learning approach has been extensively studied across various problems, such as image classification, video classification, information extraction, and text classification, to name only a few.

Algorithm 1 Steps of the Proposed EGPC-based PLA Scheme

Input: \mathcal{U} : unlabeled fingerprint samples $\{x^{(u)}\}_{u=1}^U$; \mathcal{L} : initially labeled fingerprint samples $\{\langle x, y \rangle\}_{l=1}^L$ **Process:**

- 1: **for** $t = 1, 2, \dots$ **do**
- 2: Training the authentication system θ through the GPC-based scheme in Section III;
- 3: Selecting $x^* \in \mathcal{U}$ based on **Algorithm 2/3**;
- 4: Query the upper-layer security methods to obtain the identity of x^* , that is, label y^* ;
- 5: Add $\langle x^*, y^* \rangle$ to \mathcal{L} ;
- 6: Remove x^* from \mathcal{U}
- 7: **end for**

Output: The trained authentication system

Remark 1. For the training of SL-based PLA models, it is challenging to obtain enough labeled fingerprint samples in actual communications. This motivates us to use active learning to train a more efficient PLA model with fewer labeled training fingerprint samples. The steps of the proposed

EGPC-based PLA scheme are illustrated in **Algorithm 1**. In practice, the purpose of PLA is not taking the place of the upper-layers identity mechanisms. Instead, it is designed to complement the existing identification methods used in the upper layers, thereby enhancing the overall security level [9], [15]. In the proposed active learning-based PLA scheme, the designed fingerprint select query employs specific strategies to choose unlabeled fingerprints for annotation, and the upper-layer authentication mechanisms label the selected fingerprints x_* . The authentication model dynamically adjusts its parameters upon receiving new labeled fingerprint samples and the learning process continues until the desired authentication accuracy is reached. Hence, the designed lightweight cross-layer identification scheme can enhance the efficiency of identity recognition and provide a higher security level. Most importantly, the choice of x_* influences the training efficiency of the PLA model. In the following content, we will introduce how to choose the most uncertain fingerprint sample x_* from the \mathcal{U} of unlabeled fingerprint samples.

B. The EGPC-based PLA with RO

In each iteration, the optimal x_* is selected through optimizing an acquisition function that is usually related to $\pi(\mathbf{f}|X, \mathbf{y})$.

The Optimal Bayesian Classifier (OBC) [41] is represented by $\psi_{\pi(\mathbf{f})}(\cdot)$. The expected authentication error of the OBC can be denoted as

$$\begin{aligned} & \mathbb{E}_{\mathbf{x}_s} \{1 - p(y_s = \psi_{\pi(\mathbf{f})}(\mathbf{x}_s) | \mathbf{x}_s)\} \\ &= \mathbb{E}_{\mathbf{x}_s} \left\{1 - \max_{y_s} p(y_s | \mathbf{x}_s)\right\} \end{aligned} \quad (25)$$

For the EGPC-based PLA with RO, we first randomly sample fingerprint set $\mathcal{X}_* \subset \mathcal{X}$ with the size of M_1 , calculate the acquisition function, and then choose the fingerprint sample as the optimal x_* . Define $U^A(x_*) = \mathbb{E}_{\mathbf{x}_s} \{g^A(\mathbf{x}_s; x_*)\}$ and $U^S(x_*) = \mathbb{E}_{\mathbf{x}_s} \{g^S(\mathbf{x}_s; x_*)\}$. We denote either $g^A(\mathbf{x}_s; x_*)$ or $g^S(\mathbf{x}_s; x_*)$ by $g(\mathbf{x}_s; x_*)$ that can be calculated if we know $p(y_s | \mathbf{x}_s)$ and $p(y_s | \mathbf{x}_s, x_*, y_*)$. Through iteratively retraining the GPC-based authentication model by the EP method, the acquisition function is optimized. The training process of the designed EGPC-based PLA with RO is shown in **Algorithm 2**.

C. The EGPC-based PLA with (S)ALU

Remark 2. There are two issues for **Algorithm 2** in actual communications as follows. 1) The number of fingerprints M_2 is large to guarantee the highly-reliable approximation of the integral in (26). 2) The calculation of $p(y_s | \mathbf{x}_s, x_*, y_*)$ relies on retraining the GPC-based PLA model, which has high computational complexity $O(M_1 n^3)$. To address these two problems, we propose the EGPC-based PLA with (S)ALU, which 1) reduces the required number of fingerprint samples through importance sampling, and 2) avoids the retraining of the GPC-based models through the joint distribution calculation.

Algorithm 2 Steps of the Proposed RO-based Fingerprint Selecting Algorithm

Input: $p(\mathbf{x}); q(\mathbf{f}|X, \mathbf{y})$

Process:

- 1: Sampling M_1 fingerprint samples of $\mathbf{x}_* \sim p(\mathbf{x})$, and sampling M_2 fingerprint samples of $\mathbf{x}_s \sim p(\mathbf{x})$
 - 2: **for** each $\mathbf{x}_* \mathbf{do}$
 - 3: Calculating $p(y_*|\mathbf{x}_*)$ by (24)
 - 4: **for** y_* in $\{0, 1\}$ **do**
 - 5: Approximating the posterior $q(\mathbf{f}|\mathbf{x}_*, y_*)$ by (21), (22), and (23)
 - 6: **for** each $\mathbf{x}_s \mathbf{do}$
 - 7: Calculating $p(y_s|\mathbf{x}_s)$ and $p(y_s|\mathbf{x}_s, \mathbf{x}_*, y_*)$ by (24)
 - 8: Calculating $g(\mathbf{x}_s; \mathbf{x}_*)$
 - 9: **end for**
 - 10: **end for**
 - 11: $U(\mathbf{x}_*) = \frac{1}{M_2} \sum_{\mathbf{x}_s} g(\mathbf{x}_s; \mathbf{x}_*)$
 - 12: **end for**
- Output:** $\tilde{\mathbf{x}} = \arg \max_{\mathbf{x}_*} U(\mathbf{x}_*)$
-

Definition 2. Motivated by Mean objective Cost of Uncertainty (MOCU) [42], we define ALU as the expected loss difference between the OBC and the optimal classifier as

$$\begin{aligned} \mathcal{A}(\pi(\mathbf{f})) &\triangleq \mathbb{E}_{\mathbf{x}_s} \left\{ 1 - \max_{y_s} p(y_s|\mathbf{x}_s) \right\} \\ &- \mathbb{E}_{\pi(\mathbf{f})} \left\{ \mathbb{E}_{\mathbf{x}_s} \left[1 - \max_{y_s} p(y_s|\mathbf{x}_s, \mathbf{f}) \right] \right\} \end{aligned} \quad (26)$$

The ALU reduction can be taken as the acquisition function as

$$U^A(\mathbf{x}_*; \pi(\mathbf{f})) = \mathcal{A}(\pi(\mathbf{f})) - \mathbb{E}_{y_*|\mathbf{x}_*} [\mathcal{A}(\pi(\mathbf{f}|\mathbf{x}_*, y_*))] \quad (27)$$

According to [43], we can obtain

$$\begin{aligned} U(\mathbf{x}_*) &= \mathbb{E}_{\mathbf{x}_s} \left\{ 1 - \max_{y_s} p(y_s|\mathbf{x}_s) \right\} \\ &- \mathbb{E}_{y_*|\mathbf{x}_*} \left\{ \mathbb{E}_{\mathbf{x}_s} [1 - \max_{y_s} p(y_s|\mathbf{x}_s, \mathbf{x}_*, y_*)] \right\} \\ &= \mathbb{E}_{\mathbf{x}_s} \left\{ \mathbb{E}_{y_*|\mathbf{x}_*} \left[\max_{y_s} p(y_s|\mathbf{x}_s, \mathbf{x}, y) \right] - \max_{y_s} p(y_s|\mathbf{x}_s) \right\} \end{aligned} \quad (28)$$

which is also the Expected Error Reduction (EER) of OBC [44].

Definition 3. Inspired by Soft-MOCU [45], we define SALU in (29), which has a smooth concave approximation of ALU.

$$\begin{aligned} \mathcal{A}^S(\pi(\mathbf{f})) &\triangleq \mathbb{E}_{\mathbf{x}_s} \left\{ 1 - \frac{1}{k} \text{LogSumExp}(k \cdot p(y_s|\mathbf{x}_s)) \right\} \\ &- \mathbb{E}_{\pi(\mathbf{f})} \left\{ \mathbb{E}_{\mathbf{x}_s} [1 - \max_{y_s} p(y_s|\mathbf{x}_s, \mathbf{f})] \right\} \end{aligned} \quad (29)$$

The corresponding acquisition function is denoted as

$$\begin{aligned} U^S(\mathbf{x}_*) &= \mathbb{E}_{\mathbf{x}_s} \left\{ \mathbb{E}_{y_*|\mathbf{x}_*} \left[\frac{1}{k} \log \text{SumExp}(k \cdot p(y_s | \mathbf{x}_s, \mathbf{x}_*, y_*)) \right] \right. \\ &\left. - \frac{1}{k} \log \text{SumExp}(k \cdot p(y_s | \mathbf{x}_s)) \right\} \end{aligned} \quad (30)$$

which has no maximization operators.

Algorithm 3 Steps of the Proposed (S)ALU-based Fingerprint Selecting Algorithms

Input: $p(\mathbf{x}); q(\mathbf{f}|X, \mathbf{y})$

Process:

- 1: Sample M_1 fingerprint samples of $\mathbf{x}_* \sim p(\mathbf{x})$
 - 2: **for** each $\mathbf{x}_* \mathbf{do}$
 - 3: Calculate $p(y_*|\mathbf{x}_*)$ by (24)
 - 4: Sample M_2 fingerprint samples of $\mathbf{x}_s \sim \tilde{p}(\mathbf{x}_s; \mathbf{x}_*)$
 - 5: **for** y_* in $\{0, 1\}$ **do**
 - 6: **for** each $\mathbf{x}_s \mathbf{do}$
 - 7: Calculate $p(y_s|\mathbf{x}_s, \mathbf{x}_*, y_*)$ by (33)
 - 8: Calculate $p(y_s|\mathbf{x}_s)$ by (24)
 - 9: Calculate $p(y_s|\mathbf{x}_s, \mathbf{x}_*, y_*) = \frac{p(y_s, y_*|\mathbf{x}_s, \mathbf{x}_*)}{p(y_s|\mathbf{x}_s)}$
 - 10: Calculate $g(\mathbf{x}_s; \mathbf{x}_*)$
 - 11: **end for**
 - 12: **end for**
 - 13: $U(\mathbf{x}_*) = \frac{1}{M_2} \sum_{\mathbf{x}_s} \frac{p(\mathbf{x}_s)g(\mathbf{x}_s; \mathbf{x}_*)}{\tilde{p}(\mathbf{x}_s; \mathbf{x}_*)}$
 - 14: **end for**
- Output:** $\tilde{\mathbf{x}} = \arg \max_{\mathbf{x}_*} U(\mathbf{x}_*)$
-

1) *Importance Sampling:* $U(\mathbf{x}_*)$ in (28) can be reformulated over the distribution $\tilde{p}(\mathbf{x}_s; \mathbf{x}_*)$ as

$$U(\mathbf{x}_*) = \mathbb{E}_{\mathbf{x}_s \sim \tilde{p}(\mathbf{x}_s; \mathbf{x}_*)} \left[\frac{p(\mathbf{x}_s)g(\mathbf{x}_s; \mathbf{x}_*)}{\tilde{p}(\mathbf{x}_s; \mathbf{x}_*)} \right] \quad (31)$$

Assuming $\tilde{p}(\mathbf{x}_s; \mathbf{x}_*) \propto k(\mathbf{x}_s; \mathbf{x}_*)p(\mathbf{x}_s)$, we can obtain $p(y_s|\mathbf{x}_s, \mathbf{x}_*, y_*) \approx 0$ and $g(\mathbf{x}_s; \mathbf{x}_*) \approx 0$.

2) *Joint Distribution Calculation:* To address the second issue in Remark 2, $p(y_s|\mathbf{x}_s, \mathbf{x}_*, y_*)$ is obtained as

$$p(y_s|\mathbf{x}_s, \mathbf{x}_*, y_*) = \frac{p(y_s, y_*|\mathbf{x}_s, \mathbf{x}_*)}{p(y_*|\mathbf{x}_*)} \quad (32)$$

The calculation requires $p(y_s, y_*|\mathbf{x}_s, \mathbf{x}_*)$.

Proposition 7. The joint distribution $p(y_s, y_*|\mathbf{x}_s, \mathbf{x}_*)$ is expressed as

$$\begin{aligned} p(y_s = 1, y_* = 1|\mathbf{x}_s, \mathbf{x}_*) &= \int \Phi \left(\frac{\tilde{\mu}_*(f_s)}{\sqrt{\tilde{\sigma}_{**} + 1}} \right) \Phi(f_s) \phi(f_s|\mu_s, \sigma_{ss}) df_s \end{aligned} \quad (33)$$

where $f_s = f(\mathbf{x}_s)$, $f_* = f(\mathbf{x}_*)$, μ_{s^*} and Σ_{s^*} represent the marginal mean and covariance matrices of f_s and f_* , respectively. Denoting $\mu_{s^*} = \begin{pmatrix} \mu_s \\ \mu_* \end{pmatrix}$ and $\Sigma_{s^*} = \begin{pmatrix} \sigma_{ss} & \sigma_{s*} \\ \sigma_{s*} & \sigma_{**} \end{pmatrix}$, $\phi(f_s, f_*|\mu_{s^*}, \Sigma_{s^*}) = (f_s|\mu_s, \sigma_{ss})(f_*|\tilde{\mu}_*(f_s), \tilde{\sigma}_{**})$, where $\tilde{\mu}_*(f_s) = \mu_* + \frac{(f_s - \mu_s)\sigma_{s*}}{\sigma_{ss}}$ and $\tilde{\sigma}_{**} = \sigma_{**} - \frac{\sigma_{s*}^2}{\sigma_{ss}}$.

Proof: See Appendix F. ■

The process of the proposed (S)ALU-based fingerprint selecting algorithms is shown in **Algorithm 3** in detail.

V. PERFORMANCE EVALUATION AND SIMULATION RESULTS

A. Performance Metric

1) *Authentication Error Rate:* Authentication error rate R_e is used to measure the authentication performance, which is

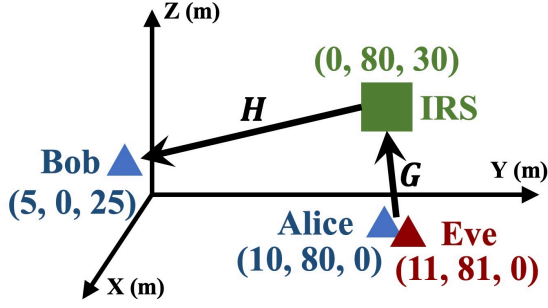


Fig. 3. The positions of Alice, Eve, Bob, and IRS.

represented as

$$R_e = \frac{1}{N_a} \sum_{n=1}^{N_a} \mathbb{I}(L_n \neq Y_n) \quad (34)$$

where N_a is the number of testing fingerprints, and L_n and Y_n respectively represent the true and estimated identities of the n th fingerprint. $\mathbb{I}(\cdot)$ takes 1 or 0 if \cdot is true or not, respectively.

2) *Error Rate Difference*: Error rate difference D_e indicates the difference between the authentication error rate R_e in perfect and imperfect channel estimation conditions, which can be denoted as

$$D_e = R_e^i - R_e^p \quad (35)$$

where R_e^i and R_e^p respectively represent the authentication error rate in perfect and imperfect channel estimation conditions.

B. Simulation Parameters

Fingerprint samples are generated through MATLAB platform, and the performance of PLA models is verified through PyCharm. The baseline algorithms include MES [46] and BALD [47].

The positions of Alice, Eve, Bob, and IRS are illustrated in Fig. 3. Alice, Eve, and Bob are equipped with Uniform linear arrays, and the number of arrays of Alice/Eve and Bob are $N_T = 2$ and $N_R = 4$, respectively. IRS is a uniform rectangular array composed of $N = N_y N_z = 8 * 32$ reflective elements, and the distance between each reflective element is half wavelength. \mathbf{H} and \mathbf{G} are modeled as Rician Channel as

$$\mathbf{H} = \sqrt{\frac{PL_H^{LoS} \kappa_H}{1 + \kappa_H}} \bar{\mathbf{H}} + \sqrt{\frac{PL_H^{NLoS}}{1 + \kappa_H}} \tilde{\mathbf{H}} \quad (36)$$

$$\mathbf{G} = \sqrt{\frac{PL_G^{LoS} \kappa_G}{1 + \kappa_G}} \bar{\mathbf{G}} + \sqrt{\frac{PL_G^{NLoS}}{1 + \kappa_G}} \tilde{\mathbf{G}} \quad (37)$$

where $\bar{\mathbf{H}}$ and $\bar{\mathbf{G}}$ are Line of Sight (LoS) paths, and $\tilde{\mathbf{H}}$ and $\tilde{\mathbf{G}}$ are Non-LoS (NLoS) paths. PL denotes the corresponding path loss, which are denoted as follows according to the 3GPP TR 38.901 [48].

$$PL_{LoS} = 32.4 + 21 \log_{10}(d) + 20 \log_{10}(f_c) \quad (38)$$

$$PL_{NLoS} = 32.4 + 31.9 \log_{10}(d) + 20 \log_{10}(f_c) \quad (39)$$

where d is the distance (in m) of the path, $f_c = 3.5$ GHz is the carrier frequency, and $\kappa_H = 3$ and $\kappa_G = 4$ are the

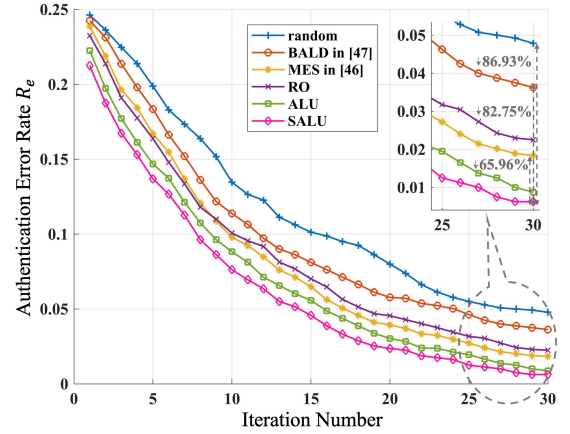


Fig. 4. Authentication error rate R_e versus different iteration numbers under the IRS-assisted wireless environment.

Rician factor. The bandwidth is 1 MHz. The LoS paths are modeled according to [49]. The NLoS paths are modeled as Rayleigh fading models, that is, each element of the channel matrix obeys the independent identically distributed variable $\mathcal{CN}(0, \mathbf{I})$. The directed channels \mathbf{D} between Alice/Eve and Bob are modeled as Rayleigh channels due to the severe decline.

The synthetic datasets are split into training and testing datasets, and the numbers of training and testing fingerprint samples per transmitter are 800 and 200, respectively. Initially two fingerprint samples are chosen from Alice and Eve for labeling and further used to estimate the GPC hyper-parameters. The learning procedures are repeated for 100 runs.

C. Simulation Results and Analysis

1) *Perfect Channel Estimation*: Based on (1), the estimated configurable fingerprint can be denoted as $\mathbf{Q}^{(A,I,B)} = \mathbf{H}\Psi\mathbf{G}$. Artificial noises $\mathbf{W} \sim \mathcal{CN}(0, \sigma_w^2 \mathbf{I})$ are added to model noisy wireless environments, where $\sigma_w^2 = 10^{-20}$.

Fig. 4 compared the proposed RO-based, ALU-based, and SALU-based PLA schemes with the PLA schemes based on random algorithm, BALD, and MES. As the iteration number increases, all of the algorithms achieve lower authentication error rate. It is because that the proposed GPC-based authentication model can observe more labeled fingerprint samples, better understand the distribution of fingerprints, and make more accurate predictions. In addition, more fingerprint samples can reduce the risk of over-fitting and make the model better generalized to unknown fingerprint. BALD does not perform well, which is because it is better at learning the characteristics of low-dimensional data. MES tends to prioritize querying points that are in close proximity to the decision boundary. However, the cascade fingerprint has multiple boundaries for multi-dimensions. The proposed ALU-based PLA scheme can take the EER as the acquisition function, thus achieving better authentication performance than the proposed RO-based PLA scheme. Compared with the ALU-based authentication method, the suggested SALU-based approach can obtain lower error rate due to smoother concave approximation. Fig. 4 demonstrates the superiority of the suggested ALU-based and SALU-based PLA schemes

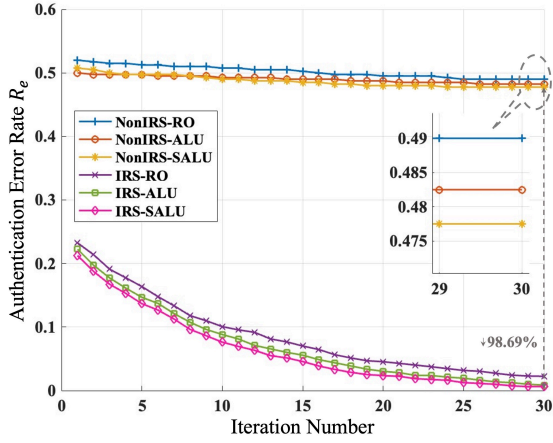


Fig. 5. Authentication error rate R_e versus different iteration numbers under non-IRS and IRS-assisted wireless environments.

than baseline algorithms in sampling efficiency of fingerprint samples.

Fig. 5 presents the authentication performance under non-IRS and IRS-assisted wireless environments. Regardless of the iteration numbers, the authentication error rate of all the proposed schemes under non-IRS scenarios is always around 0.5. Due to the severe decline of Rayleigh channels, it is challenging to effectively learn the inherent characteristics of fingerprints. In contrast, the created transmission path by IRS has better channel quality, which is modeled as cascade Rician channels. Therefore, the proposed schemes can obtain much better authentication performance with the help of IRS. Fig. 5 shows the effectiveness of IRS in enhancing authentication performance compared with the conventional non-IRS-based PLA framework under low SNR environments.

Fig. 6 further provides the authentication performance versus different phase parameters of the IRS element $\theta = \theta_1 = \theta_2 = \dots = \theta_n$, where θ_n is the phase parameter of the n th IRS element. With the increase of the phase, the authentication error rate fluctuates with different amplitude. Fig. 6 verifies that the choice of phase parameters of IRS has influences on the authentication performance. However, the optimization of IRS parameters is another important research area, and it is difficult to draw obvious conclusions about phase parameters of IRS and authentication error rate according to Fig. 6.

Fig. 7 compares the authentication performance versus different numbers of columns of IRS N_z . As the number of columns of IRS increases, the number of IRS element $N = N_y N_z$ increases. Therefore, the dimension of \mathbf{H} , $\mathbf{\Psi}$, and \mathbf{G} in the cascade channel matrix $\mathbf{Q}^{(A,I,B)} = \mathbf{H}\mathbf{\Psi}\mathbf{G}$ increases. When the dimension of \mathbf{H} , $\mathbf{\Psi}$, and \mathbf{G} is small, the limited range of the particular fingerprint distribution may not be enough to always distinguish transmitters. In contrast, when the dimension of \mathbf{H} , $\mathbf{\Psi}$, and \mathbf{G} is large, it is more difficult for attackers to successfully predict or imitate each dimension component of fingerprints.

2) *Imperfect Channel Estimation*: Imperfect CSI models are denoted as $\mathbf{H} = \mathbf{H}_i \odot \mathbf{H}_e$ and $\mathbf{G} = \mathbf{G}_i \odot \mathbf{G}_e$, where \mathbf{H}_i and \mathbf{G}_i are ideal CSI matrices, \odot denotes the hadamard product, and \mathbf{H}_e and \mathbf{G}_e are error matrices, which are represented respectively as $\mathbf{H}_e \sim \mathcal{CN}(\mathbf{I}, \sigma_H^2 \mathbf{I})$ and $\mathbf{G}_e \sim \mathcal{CN}(\mathbf{I}, \sigma_G^2 \mathbf{I})$.

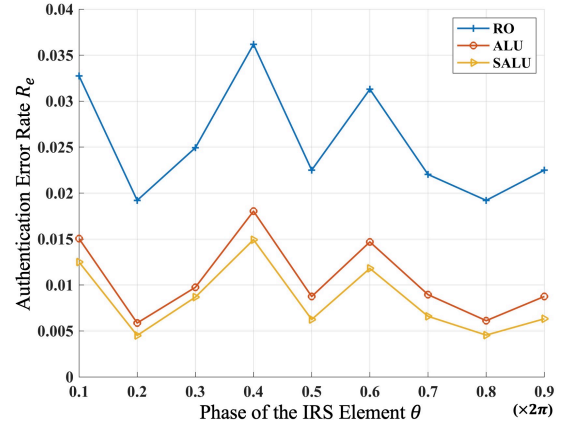


Fig. 6. Authentication error rate R_e versus different phase parameters of the IRS element θ .

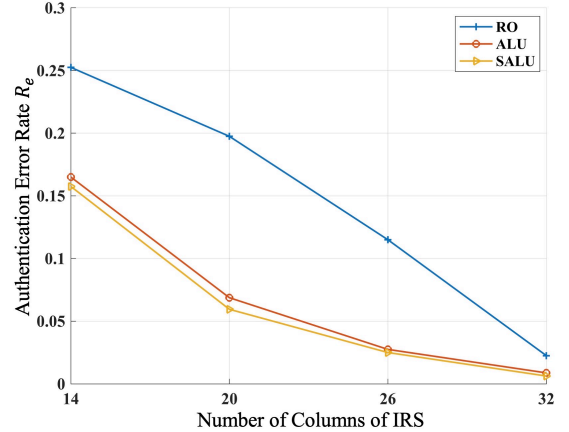


Fig. 7. Authentication error rate R_e versus different numbers of columns of IRS N_z .

Fig. 8 illustrates the authentication performance versus different Channel estimation errors. When $\sigma^2 \leq 8$, all of the schemes are robust of channel estimation errors. It can be explained that, due to the assistance of IRS, the configurable fingerprints of different transmitters are easy to distinguish. When $\sigma^2 = 9$, only the random sampling-based scheme has higher authentication error rate than that in perfect channel estimation condition. When $\sigma^2 \geq 10$, as σ^2 increases, the authentication performance is gradually declining. Nevertheless, the proposed ALU-based and SALU-based schemes can achieve lower authentication error rate than baseline schemes. In addition, the proposed SALU-based scheme always has the best authentication performance than the other schemes. Fig. 8 verifies the robustness of the proposed (S)ALU-based PLA schemes to channel estimation errors.

Fig. 9 uses the computational time as a metric to demonstrate the complexity of PLA schemes. Because of the retraining of the GPC-based authentication model for every $(\mathbf{x}_*, \mathbf{y}_*)$, the proposed RO-based scheme has the highest complexity. In contrast, through the importance sampling in (31) and joint distribution calculation in (32), the proposed (S)ALU-based schemes can accelerate the authentication process. In comparison to the proposed ALU-based scheme, the designed SALU-based PLA scheme demands additional training time to achieve a lower authentication error rate.

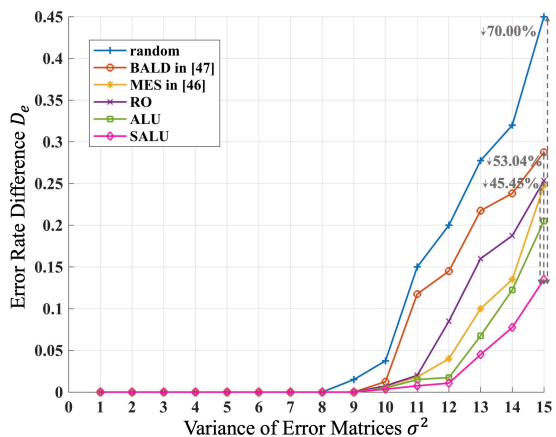


Fig. 8. Error rate difference D_e under the IRS-assisted wireless environment versus different variance of error matrices $\sigma^2 = \sigma_H^2 = \sigma_C^2$.

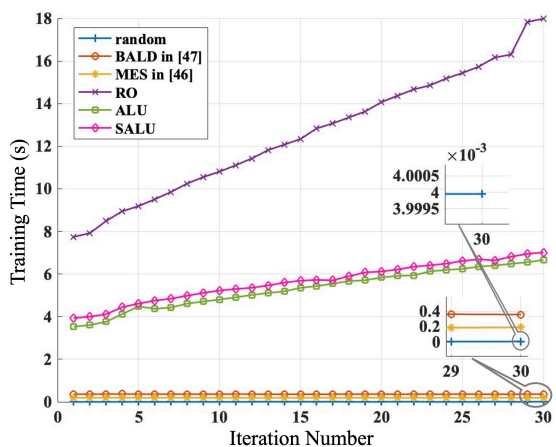


Fig. 9. Training time versus different iteration numbers under the IRS-assisted wireless environment.

VI. CONCLUSION

To enhance wireless identity security in the context of 6G-enabled Internet of Things (IoT), we introduce a configurable-fingerprint-based PLA framework utilizing IRS. Compared with the non-IRS-based PLA approaches, the designed IRS-assisted method can improve the discrimination of fingerprints through creating an alternative transmission path. We further suggest a GPC-based PLA scheme and provide the closed mathematical expression of posterior prediction of identity of unknown fingerprints. Considering that the labels of fingerprints are difficult to obtain in actual scenarios, we further combine active learning and the GPC-based PLA to propose three EGPC-based PLA schemes, which requires much fewer labeled fingerprints and has more universality.

Through simulations performed on synthetic datasets, we validate the superiority of our IRS-assisted PLA approach over non-IRS-based framework in low SNR environments. Additionally, we demonstrate that our proposed EGPC-based approaches outperform baseline algorithms. Furthermore, the simulation results indicate that adjusting the parameters of IRS, such as the number and phase parameters of IRS elements, can further reduce the authentication error rate. It is important to highlight that the optimization of phase parameters in IRSs is a topic that necessitates further exploration,

which will be studied using RL methods in future research.

APPENDIX A THE PROOF OF PROPOSITION 2

For the jointly Gaussian random vectors \mathbf{x} and \mathbf{y} , we have

$$\begin{aligned} \begin{bmatrix} \mathbf{x} \\ \mathbf{y} \end{bmatrix} &\sim \mathcal{N} \left(\begin{bmatrix} \boldsymbol{\mu}_x \\ \boldsymbol{\mu}_y \end{bmatrix}, \begin{bmatrix} A & C \\ C^T & B \end{bmatrix} \right) \\ &= \mathcal{N} \left(\begin{bmatrix} \boldsymbol{\mu}_x \\ \boldsymbol{\mu}_y \end{bmatrix}, \begin{bmatrix} \tilde{A} & \tilde{C} \\ \tilde{C}^T & B \end{bmatrix}^{-1} \right) \end{aligned} \quad (40)$$

then the marginal and conditional distribution of \mathbf{x} are shown as follows according to [40].

$$\mathbf{x} \sim \mathcal{N}(\boldsymbol{\mu}_x, A) \quad (41)$$

$$\mathbf{x}|\mathbf{y} \sim \mathcal{N}(\boldsymbol{\mu}_x + CB^{-1}(\mathbf{y} - \boldsymbol{\mu}_y), A - CB^{-1}C^T) \quad (42)$$

$$\mathbf{x}|\mathbf{y} \sim \mathcal{N}(\boldsymbol{\mu}_x - \tilde{A}^{-1}\tilde{C}(\mathbf{y} - \boldsymbol{\mu}_y), \tilde{A}^{-1}) \quad (43)$$

Thus, **Proposition 2** is proved.

APPENDIX B THE PROOF OF PROPOSITION 3

The product of two Gaussian distributions is represented as

$$\mathcal{N}(\mathbf{x}|\mathbf{a}, A)\mathcal{N}(\mathbf{x}|\mathbf{b}, B) = Z^{-1}\mathcal{N}(\mathbf{x}|\mathbf{c}, C) \quad (44)$$

where

$$\mathbf{c} = C(A^{-1}\mathbf{a} + B^{-1}\mathbf{b}) \quad (45)$$

$$C = (A^{-1} + B^{-1})^{-1} \quad (46)$$

$$Z^{-1} = (2\pi)^{-\frac{D}{2}} |A + B|^{-\frac{1}{2}} \exp \left(-\frac{(\mathbf{a} - \mathbf{b})^T (\mathbf{a} - \mathbf{b})}{2(A + B)} \right) \quad (47)$$

Thus, through multiplying the cavity distribution by t_i from (11), **Proposition 3** is proved.

APPENDIX C THE PROOF OF PROPOSITION 4

Consider

$$Z = \int_{-\infty}^{\infty} \Phi \left(\frac{x - m}{v} \right) \mathcal{N}(x|\mu, \sigma^2) dx \quad (48)$$

When $v > 0$, by combining $z = y - x + \mu - m$ and $w = x - \mu$ we can get

$$\begin{aligned} Z_{v>0} &= \frac{\int_{-\infty}^{\infty} \int_{-\infty}^{\infty} \exp \left(-\frac{(y-m)^2}{2v^2} - \frac{(x-\mu)^2}{2\sigma^2} \right) dy dx}{2\pi\sigma v} \\ &= \frac{\int_{-\infty}^{\mu-m} \int_{-\infty}^{\infty} \exp \left(-\frac{(z+w)^2}{2v^2} - \frac{w^2}{2\sigma^2} \right) dw dz}{2\pi\sigma v} \end{aligned} \quad (49)$$

$$\begin{aligned} Z_{v>0} &= \frac{\int_{-\infty}^{\mu-m} \int_{-\infty}^{\infty} \exp \left(-\frac{1}{2} \begin{bmatrix} w \\ z \end{bmatrix}^T \begin{bmatrix} \frac{1}{v^2} + \frac{1}{\sigma^2} & \frac{1}{v^2} \\ \frac{1}{v^2} & \frac{1}{v^2} \end{bmatrix} \begin{bmatrix} w \\ z \end{bmatrix} \right) dw dz}{2\pi\sigma v} \\ &= \int_{-\infty}^{\mu-m} \int_{-\infty}^{\infty} \mathcal{N} \left(\begin{bmatrix} w \\ z \end{bmatrix} \middle| \mathbf{0}, \begin{bmatrix} \sigma^2 & -\sigma^2 \\ -\sigma^2 & v^2 + \sigma^2 \end{bmatrix} \right) dw dz \end{aligned} \quad (50)$$

According to (42) and (43), we can get

$$Z_{v>0} = \frac{\int_{-\infty}^{\mu-m} \exp\left(-\frac{z^2}{2(v^2+\sigma^2)}\right) dz}{\sqrt{2\pi(v^2+\sigma^2)}} = \Phi\left(\frac{\mu-m}{\sqrt{v^2+\sigma^2}}\right) \quad (51)$$

When $v < 0$, by combining $\Phi(-z) = 1 - \Phi(z)$ and (48),

$$Z_{v<0} = 1 - \Phi\left(\frac{\mu-m}{\sqrt{v^2+\sigma^2}}\right) = \Phi\left(-\frac{\mu-m}{\sqrt{v^2+\sigma^2}}\right) \quad (52)$$

By collecting (51) and (52), we can get

$$Z = \int \Phi\left(\frac{x-m}{v}\right) \mathcal{N}(x|\mu, \sigma^2) dx = \Phi(z) \quad (53)$$

where $z = \frac{\mu-m}{v\sqrt{1+\sigma^2/v^2}}$ ($v \neq 0$). By differentiating with respect to μ on (53), we can obtain

$$\begin{aligned} \frac{\partial Z}{\partial \mu} &= \int \frac{x-\mu}{\sigma^2} \Phi\left(\frac{x-m}{v}\right) \mathcal{N}(x|\mu, \sigma^2) dx = \frac{\partial}{\partial \mu} \Phi(z) \\ &\iff \frac{1}{\sigma^2} \int x \Phi\left(\frac{x-m}{v}\right) \mathcal{N}(x|\mu, \sigma^2) dx - \frac{\mu Z}{\sigma^2} \\ &= \frac{\mathcal{N}(z)}{v\sqrt{1+\sigma^2/v^2}} \end{aligned} \quad (54)$$

where $\partial\Phi(z)/\partial\mu = \mathcal{N}(z)\partial z/\partial\mu$ is utilized. Multiplying through by σ^2/Z , (55) is obtained.

$$\mathbb{E}_q[x] = \mu + \frac{\sigma^2 \mathcal{N}(z)}{\Phi(z) v \sqrt{1 + \frac{\sigma^2}{v^2}}} \quad (55)$$

Similarly, we can obtain the second moment as

$$\begin{aligned} \frac{\partial^2 Z}{\partial \mu^2} &= \int \left[\frac{x^2}{\sigma^4} - \frac{2\mu x}{\sigma^4} + \frac{\mu^2}{\sigma^4} - \frac{1}{\sigma^2}\right] \Phi\left(\frac{x-m}{v}\right) \mathcal{N}(x|\mu, \sigma^2) dx \\ &= -\frac{z\mathcal{N}(z)}{v^2 + \sigma^2} \iff \\ \mathbb{E}_q[x^2] &= 2\mu\mathbb{E}_q[x] - \mu^2 + \sigma^2 - \frac{\sigma^4 z \mathcal{N}(z)}{\Phi(z)(v^2 + \sigma^2)} \end{aligned} \quad (56)$$

By combining (55) and (56), we can get

$$\begin{aligned} \mathbb{E}_q\left[(x - \mathbb{E}_q[x])^2\right] &= \mathbb{E}_q[x^2] - \mathbb{E}_q[x]^2 \\ &= \sigma^2 - \frac{\sigma^4 \mathcal{N}(z)}{(v^2 + \sigma^2) \Phi(z)} \left(z + \frac{\mathcal{N}(z)}{\Phi(z)}\right) \end{aligned} \quad (57)$$

Thus, **Proposition 4** is proved.

APPENDIX D THE PROOF OF PROPOSITION 5

We can obtain (21), (22), and (23) according to (45), (46), and (47). Hence, **Proposition 5** is proved.

APPENDIX E THE PROOF OF PROPOSITION 6

The approximated mean for f_* can be denoted as

$$\begin{aligned} \mathbb{E}_q[f_*|X, \mathbf{y}, \mathbf{x}_*] &= \mathbf{k}_*^T K^{-1} \boldsymbol{\mu} \\ &= \mathbf{k}_*^T K^{-1} \left(K^{-1} + \tilde{\Sigma}^{-1}\right)^{-1} \tilde{\Sigma}^{-1} \tilde{\boldsymbol{\mu}} \\ &= \mathbf{k}_*^T \left(K + \tilde{\Sigma}\right)^{-1} \tilde{\boldsymbol{\mu}} \end{aligned} \quad (58)$$

The variance of $f_*|(X, \mathbf{y})$ under the Gaussian approximation can be denoted as

$$\begin{aligned} \mathbb{V}_q[f_*|X, \mathbf{y}, \mathbf{x}_*] &= \mathbb{E}_{p(f_*|X, \mathbf{x}_*, \mathbf{f})} f_*^2 - \mathbb{E}[f_*|X, \mathbf{x}_*, \mathbf{f}]^2 \\ &= k(\mathbf{x}_*, \mathbf{x}_*) - \mathbf{k}_*^T K^{-1} \mathbf{k}_* + \mathbf{k}_*^T K^{-1} \left(K^{-1} + \tilde{\Sigma}\right)^{-1} K^{-1} \mathbf{k}_* \\ &= k(\mathbf{x}_*, \mathbf{x}_*) - \mathbf{k}_*^T \left(K^{-1} + \tilde{\Sigma}\right)^{-1} \mathbf{k}_* \end{aligned} \quad (59)$$

Then, we can obtain

$$\begin{aligned} q(y_*|X, \mathbf{y}, \mathbf{x}_*) &= \mathbb{E}_q[\pi_*|X, \mathbf{y}, \mathbf{x}_*] \\ &= \int \Phi(f_*) q(f_*|X, \mathbf{y}, \mathbf{x}_*) df_* \end{aligned} \quad (60)$$

According to (51), we can obtain

$$\begin{aligned} q(y_*|X, \mathbf{y}, \mathbf{x}_*) &= \Phi\left(\frac{\mathbf{k}_*^T \left(K + \tilde{\Sigma}\right)^{-1} \tilde{\boldsymbol{\mu}}}{\sqrt{1 + k(\mathbf{x}_*, \mathbf{x}_*) - \mathbf{k}_*^T \left(K + \tilde{\Sigma}\right)^{-1} \mathbf{k}_*}}\right) \end{aligned} \quad (61)$$

By combining (13) and (61), **Proposition 6** is proved.

APPENDIX F THE PROOF OF PROPOSITION 7

Given f_s and f_* , y_s and y_* are conditionally independent. Hence, $p(y_s, y_*|\mathbf{x}_s, \mathbf{x}_*)$ can be represented as

$$\begin{aligned} p(y_s = 1, y_* = 1|\mathbf{x}_s, \mathbf{x}_*) &= \iint \Phi(f_s) \Phi(f_*) \phi(f_s, f_*|\mu_{s*}, \Sigma_{s*}) df_s df_* \\ &= \iint \Phi(f_*) \phi(f_*|\tilde{\mu}_*(f_s), \tilde{\sigma}_{**}) df_* \Phi(f_s) \phi(f_s|\mu_s, \sigma_{ss}) df_s \\ &= \int \Phi\left(\frac{\tilde{\mu}_*(f_s)}{\sqrt{\tilde{\sigma}_{**} + 1}}\right) \Phi(f_s) \phi(f_s|\mu_s, \sigma_{ss}) df_s \end{aligned} \quad (62)$$

Hence, **Proposition 7** is proved.

REFERENCES

- [1] J. Wang, M. K. Lim, C. Wang, and M.-L. Tseng, "The evolution of the internet of things (iot) over the past 20 years," *Comput. Ind. Eng.*, vol. 155, p. 107174, 2021.
- [2] D. C. Nguyen, M. Ding, P. N. Pathirana, A. Seneviratne, J. Li, D. Niyato, O. Dobre, and H. V. Poor, "6g internet of things: A comprehensive survey," *IEEE Internet Things J.*, vol. 9, no. 1, pp. 359–383, 2022.
- [3] Z. Zhang, Y. Xiao, Z. Ma, M. Xiao, Z. Ding, X. Lei, G. K. Karagiannidis, and P. Fan, "6g wireless networks: Vision, requirements, architecture, and key technologies," *IEEE Veh. Technol. Mag.*, vol. 14, no. 3, pp. 28–41, 2019.
- [4] S. Dang, O. Amin, B. Shihada, and M.-S. Alouini, "What should 6g be?" *Nat. Electron.*, vol. 3, no. 1, pp. 20–29, 2020.

- [5] P. Yang, Y. Xiao, M. Xiao, and S. Li, "6g wireless communications: Vision and potential techniques," *IEEE Netw.*, vol. 33, no. 4, pp. 70–75, 2019.
- [6] S. Xia, X. Tao, N. Li, S. Wang, T. Sui, H. Wu, J. Xu, and Z. Han, "Multiple correlated attributes based physical layer authentication in wireless networks," *IEEE Trans. Veh. Technol.*, vol. 70, no. 2, pp. 1673–1687, 2021.
- [7] S. R. Garzon, H. Yildiz, and A. Küpper, "Decentralized identifiers and self-sovereign identity in 6g," *IEEE Netw.*, vol. 36, no. 4, pp. 142–148, 2022.
- [8] 3GPP, "Security architecture and procedures for 5g system, version 17.0.0," 2020.
- [9] N. Xie, J. Zhang, and Q. Zhang, "Security provided by the physical layer in wireless communications," *IEEE Netw.*, 2022.
- [10] C. Cheng, R. Lu, A. Petzoldt, and T. Takagi, "Securing the internet of things in a quantum world," *IEEE Commun. Mag.*, vol. 55, no. 2, pp. 116–120, 2017.
- [11] I. H. Abdulqadder and S. Zhou, "Sliceblock: context-aware authentication handover and secure network slicing using dag-blockchain in edge-assisted sdn/nfv-6g environment," *IEEE Internet Things J.*, vol. 9, no. 18, pp. 18 079–18 097, 2022.
- [12] H. Fang, X. Wang, and L. Hanzo, "Learning-aided physical layer authentication as an intelligent process," *IEEE Trans. Commun.*, vol. 67, no. 3, pp. 2260–2273, 2018.
- [13] H. Fang, X. Wang, and S. Tomasin, "Machine learning for intelligent authentication in 5g and beyond wireless networks," *IEEE Wirel. Commun.*, vol. 26, no. 5, pp. 55–61, 2019.
- [14] L. Jin, X. Hu, Y. Lou, Z. Zhong, X. Sun, H. Wang, and J. Wu, "Introduction to wireless endogenous security and safety: Problems, attributes, structures and functions," *China Commun.*, vol. 18, no. 9, pp. 88–99, 2021.
- [15] N. Xie, Z. Li, and H. Tan, "A survey of physical-layer authentication in wireless communications," *IEEE Commun. Surv. Tutor.*, vol. 23, no. 1, pp. 282–310, 2020.
- [16] R. Meng, X. Xu, B. Wang, H. Sun, S. Xia, S. Han, and P. Zhang, "Physical-layer authentication based on hierarchical variational autoencoder for industrial internet of things," *IEEE Internet Things J.*, vol. 10, no. 3, pp. 2528–2544, 2022.
- [17] R. Meng, X. Xu, H. Sun, H. Zhao, B. Wang, S. Han, and P. Zhang, "Multiuser physical-layer authentication based on latent perturbed neural networks for industrial internet of things," *IEEE Internet Things J.*, vol. 10, no. 1, pp. 637–652, 2022.
- [18] R. Meng, X. Xu, H. Zhao, B. Wang, G. Li, B. Xu, and P. Zhang, "Multi-observation-multi-channel-attribute-based multiuser authentication for industrial wireless edge networks," *IEEE Trans. Ind. Inform.*, 2023.
- [19] L. Senigagliales, M. Baldi, and E. Gambi, "Authentication at the physical layer with cooperative communications and machine learning," in *2022 Joint European Conference on Networks and Communications & 6G Summit (EuCNC/6G Summit)*. IEEE, 2022, pp. 71–76.
- [20] R.-F. Liao, H. Wen, S. Chen, F. Xie, F. Pan, J. Tang, and H. Song, "Multiuser physical layer authentication in internet of things with data augmentation," *IEEE Internet Things J.*, vol. 7, no. 3, pp. 2077–2088, 2019.
- [21] V.-L. Nguyen, P.-C. Lin, B.-C. Cheng, R.-H. Hwang, and Y.-D. Lin, "Security and privacy for 6g: A survey on prospective technologies and challenges," *IEEE Commun. Surv. Tutor.*, vol. 23, no. 4, pp. 2384–2428, 2021.
- [22] L. Xiao, L. J. Greenstein, N. B. Mandayam, and W. Trappe, "Using the physical layer for wireless authentication in time-variant channels," *IEEE Trans. Commun.*, vol. 7, no. 7, pp. 2571–2579, 2008.
- [23] D. Li, X. Yang, F. Zhou, D. Wang, and N. Al-Dhahir, "Blind physical-layer authentication based on composite radio sample characteristics," *IEEE Trans. Commun.*, vol. 70, no. 10, pp. 6790–6803, 2022.
- [24] L. Xiao, L. J. Greenstein, N. B. Mandayam, and W. Trappe, "Channel-based spoofing detection in frequency-selective rayleigh channels," *IEEE Trans. Commun.*, vol. 8, no. 12, pp. 5948–5956, 2009.
- [25] Y. Liu, P. Zhang, Y. Shen, L. Peng, and X. Jiang, "Online machine learning-based physical layer authentication for mmwave mimo systems," *Ad Hoc Networks*, vol. 131, p. 102864, 2022.
- [26] A. Chorti, A. N. Barreto, S. Köpsell, M. Zoli, M. Chafii, P. Sehier, G. Fettweis, and H. V. Poor, "Context-aware security for 6g wireless: The role of physical layer security," *IEEE Communications Standards Magazine*, vol. 6, no. 1, pp. 102–108, 2022.
- [27] H.-M. Wang and Q.-Y. Fu, "Channel-prediction-based one-class mobile iot device authentication," *IEEE Internet Things J.*, vol. 9, no. 10, pp. 7731–7745, 2021.
- [28] F. Xie, Z. Pang, H. Wen, W. Lei, and X. Xu, "Weighted voting in physical layer authentication for industrial wireless edge networks," *IEEE Trans. Ind. Inform.*, vol. 18, no. 4, pp. 2796–2806, 2021.
- [29] Y. Chen, P.-H. Ho, H. Wen, S. Y. Chang, and S. Real, "On physical-layer authentication via online transfer learning," *IEEE Internet Things J.*, vol. 9, no. 2, pp. 1374–1385, 2021.
- [30] L. Xiao, Y. Li, G. Han, G. Liu, and W. Zhuang, "Phy-layer spoofing detection with reinforcement learning in wireless networks," *IEEE Trans. Veh. Technol.*, vol. 65, no. 12, pp. 10037–10047, 2016.
- [31] F. Pan, Z. Pang, H. Wen, M. Luvisotto, M. Xiao, R.-F. Liao, and J. Chen, "Threshold-free physical layer authentication based on machine learning for industrial wireless cps," *IEEE Trans. Ind. Inform.*, vol. 15, no. 12, pp. 6481–6491, 2019.
- [32] P. Zhang, Y. Shen, X. Jiang, and B. Wu, "Physical layer authentication jointly utilizing channel and phase noise in mimo systems," *IEEE Trans. Commun.*, vol. 68, no. 4, pp. 2446–2458, 2020.
- [33] L. Xiao, X. Wan, and Z. Han, "Phy-layer authentication with multiple landmarks with reduced overhead," *IEEE Trans. Commun.*, vol. 17, no. 3, pp. 1676–1687, 2017.
- [34] M. Z. Chen, W. Tang, J. Y. Dai, J. C. Ke, L. Zhang, C. Zhang, J. Yang, L. Li, Q. Cheng, S. Jin *et al.*, "Accurate and broadband manipulations of harmonic amplitudes and phases to reach 256 qam millimeter-wave wireless communications by time-domain digital coding metasurface," *Natl. Sci. Rev.*, vol. 9, no. 1, p. nwab134, 2022.
- [35] B. Settles, *Active learning literature survey*. University of Wisconsin-Madison Department of Computer Sciences, 2009.
- [36] K. Yang, J. Ren, Y. Zhu, and W. Zhang, "Active learning for wireless iot intrusion detection," *IEEE Wirel. Commun.*, vol. 25, no. 6, pp. 19–25, 2018.
- [37] S. Tomasin, H. Zhang, A. Chorti, and H. V. Poor, "Challenge-response physical layer authentication over partially controllable channels," *IEEE Commun. Mag.*, vol. 60, no. 12, pp. 138–144, 2022.
- [38] Y. Wang, H. Lu, D. Zhao, Y. Deng, and A. Nallanathan, "Wireless communication in the presence of illegal reconfigurable intelligent surface: Signal leakage and interference attack," *IEEE Wirel. Commun.*, vol. 29, no. 3, pp. 131–138, 2022.
- [39] A. Rech, F. Moretto, and S. Tomasin, "Maximum-rate optimization of hybrid intelligent reflective surface and relay systems," in *2021 IEEE 22nd International Workshop on Signal Processing Advances in Wireless Communications (SPAWC)*. IEEE, 2021, pp. 516–520.
- [40] C. K. Williams and C. E. Rasmussen, *Gaussian processes for machine learning*. MIT press Cambridge, MA, 2006, vol. 2, no. 3.
- [41] L. A. Dalton and E. R. Dougherty, "Optimal classifiers with minimum expected error within a bayesian framework—part i: Discrete and gaussian models," *Pattern Recognit.*, vol. 46, no. 5, pp. 1301–1314, 2013.
- [42] B.-J. Yoon, X. Qian, and E. R. Dougherty, "Quantifying the objective cost of uncertainty in complex dynamical systems," *IEEE Trans. Signal Process.*, vol. 61, no. 9, pp. 2256–2266, 2013.
- [43] G. Zhao, E. Dougherty, B.-J. Yoon, F. Alexander, and X. Qian, "Efficient active learning for gaussian process classification by error reduction," *Advances in Neural Information Processing Systems*, vol. 34, pp. 9734–9746, 2021.
- [44] N. Roy and A. McCallum, "Toward optimal active learning through monte carlo estimation of error reduction," *ICML, Williamstown*, vol. 2, pp. 441–448, 2001.
- [45] G. Zhao, E. Dougherty, B.-J. Yoon, F. J. Alexander, and X. Qian, "Bayesian active learning by soft mean objective cost of uncertainty," in *International Conference on Artificial Intelligence and Statistics*. PMLR, 2021, pp. 3970–3978.
- [46] P. Sebastiani and H. P. Wynn, "Maximum entropy sampling and optimal bayesian experimental design," *Journal of the Royal Statistical Society: Series B (Statistical Methodology)*, vol. 62, no. 1, pp. 145–157, 2000.
- [47] N. Houlsby, F. Huszár, Z. Ghahramani, and M. Lengyel, "Bayesian active learning for classification and preference learning," *arXiv preprint arXiv:1112.5745*, 2011.
- [48] 3GPP, "Study on channel model for frequencies from 0.5 to 100 ghz, version 17.0.0," 2022.
- [49] X. Hu, C. Masouros, and K.-K. Wong, "Reconfigurable intelligent surface aided mobile edge computing: From optimization-based to location-only learning-based solutions," *IEEE Trans. Commun.*, vol. 69, no. 6, pp. 3709–3725, 2021.